Engineering 2015, 1(3): 384–390
DOI 10.15302/J-ENG-2015034

Research
Advanced Materials—Article

Effects of Vapor Pressure and Super-Hydrophobic Nanocomposite Coating on Microelectronics Reliability

Xuejun Fan[1,2]*, Liangbiao Chen[1], C. P. Wong[3], Hsing-Wei Chu[1], G. Q. Zhang[4,5]

ABSTRACT Modeling vapor pressure is crucial for studying the moisture reliability of microelectronics, as high vapor pressure can cause device failures in environments with high temperature and humidity. To minimize the impact of vapor pressure, a super-hydrophobic (SH) coating can be applied on the exterior surface of devices in order to prevent moisture penetration. The underlying mechanism of SH coating for enhancing device reliability, however, is still not fully understood. In this paper, we present several existing theories for predicting vapor pressure within microelectronic materials. In addition, we discuss the mechanism and effectiveness of SH coating in preventing water vapor from entering a device, based on experimental results. Two theoretical models, a micro-mechanics-based whole-field vapor pressure model and a convection-diffusion model, are described for predicting vapor pressure. Both methods have been successfully used to explain experimental results on uncoated samples. However, when a device was coated with an SH nanocomposite, weight gain was still observed, likely due to vapor penetration through the SH surface. This phenomenon may cast doubt on the effectiveness of SH coatings in microelectronic devices. Based on current theories and the available experimental results, we conclude that it is necessary to develop a new theory to understand how water vapor penetrates through SH coatings and impacts the materials underneath. Such a theory could greatly improve microelectronics reliability.

KEYWORDS vapor pressure, moisture, semiconductor reliability, microelectromechanical systems (MEMS), super-hydrophobic, nanocomposite coating

1 Introduction

As the components of microelectronic devices are produced globally in different regions, it is inevitable that microelectronics materials, such as polymeric encapsulants and die-attach thin films, would absorb a certain amount of moisture from humid ambient environments during transportation and storage. The moisture absorbed can be detrimental to device reliability, eventually causing deleterious effects such as material aging [1], hygroscopic swelling, interfacial weakening and delamination [2–4], and suppression of material strength [5–7]. Moreover, during the soldering reflow process, the entire packaged device must be exposed to very high temperatures of up to 220–270 °C. Therefore, the moisture absorbed by polymer materials in the device will experience a phase change and extremely high internal vapor pressure can be generated. As a result, the polymer material is stressed under the combined vapor pressure and thermal stress, resulting in popcorn-like failures [3].

To reduce moisture uptake and potential damage caused by high vapor pressure, surface coating can be applied to packaged devices, such as super-hydrophobic (SH) coating with nanocomposites technology [8–12]. The general rules for designing SH surfaces are: ① to minimize the surface energy and ② to increase the surface roughness. Surfaces coated with SH materials usually have excellent water-repelling properties and display a large water contact angle (> 150°) with small hysteresis (< 10°) [8, 9, 13]. Similar surfaces can be found on many natural objects, such as lotus leaves [14]. These surfaces generally combine micro and nano roughness with low free-energy coatings [15]. Although SH coating is potentially a low-cost and highly reliable microelectronic packaging solution, moisture absorption after coating was still reported [16]. The underlying mechanism of such moisture absorption, however, could not be explained by current theories of moisture transport.

In this paper, we describe the existing methods that enable the evaluation of vapor pressure within polymers, with

[1] Department of Mechanical Engineering, Lamar University, Beaumont, TX 77710, USA; [2] State Key Laboratory of Solid State Lighting, Beijing 100083, China; [3] School of Materials Science and Engineering, Georgia Tech, Atlanta, GA 30332-0245, USA; [4] Delft University of Technology, Delft 2600 AA, the Netherlands; [5] Institute of Semiconductors, Chinese Academy of Sciences, Beijing 100083, China
* Correspondence author. E-mail: xuejun.fan@lamar.edu
Received 23 June 2015; received in revised form 4 July 2015; accepted 16 September 2015

© The Author(s) 2015. Published by Engineering Sciences Press. This is an open access article under the CC BY license (http://creativecommons.org/licenses/by/4.0/)

the intention of connecting the vapor pressure of water to the effectiveness of SH coating. We also discuss the methods used to generate an SH surface, followed by a discussion of interesting absorption behaviors after SH coating under various ambient conditions.

2 Vapor pressure modeling

High vapor pressure is considered to be the dominant cause of device failures (see Figure 1 for die-attach thin-film ruptures). Modeling vapor pressure and vapor flow may also help researchers to fully understand moisture transport in materials that are coated with SH nanocomposites. Therefore, many theoretical models have been developed to address vapor pressure and the related reliability issues [17–20]. In the following discussion, we present two different approaches, both of which have been successfully used to explain experimental tests. Since vapor pressure is always associated with moisture behaviors, the relationship between vapor pressure and moisture concentration becomes the key characteristic of different vapor pressure models.

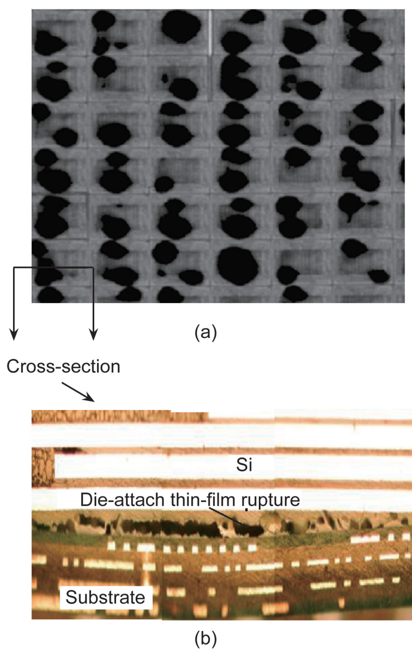

Figure 1. (a) A scanning acoustic microscopy image on a 6 × 6 array chip scale package (CSP) panel (black regions mean failures inside packages); (b) die-attach film cracking and voiding at the bottom layer where it is attached to the substrate.

2.1 Micro-mechanics-based whole-field vapor pressure model

A whole-field vapor pressure model has been developed to predict vapor pressure during soldering reflow processes, and has been successfully applied to many problems [19]. Since most microelectronic materials are typically polymer composites, the model assumes that most of the absorbed moisture collects at the voids or polymer-filler interfaces [16]. Because it has been found that the moisture density in voids can be several orders higher than the ambient moisture density, it is concluded that a liquid form of water exists within the materials [19]. Consequently, there must be two distinct states of water existing in polymers: a purely vapor phase and a mixture of liquid and vapor phases, as shown in Figure 2.

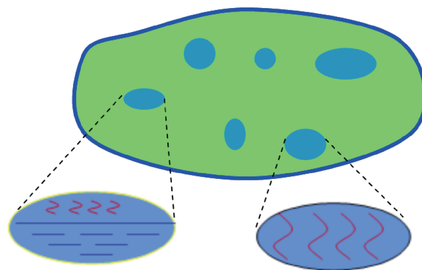

Figure 2. A schematic of a polymeric material with two different states of moisture in its pores [5].

By introducing porosity ϕ, the density (ρ) of the moisture absorbed in the materials can be calculated as

$$\rho = C/\phi \tag{1}$$

where C is moisture concentration. Moisture concentration can be obtained by solving the transient moisture diffusion equation, which is based on Fick's law and is provided here:

$$\dot{C} = -\nabla \cdot (-D\nabla C) \tag{2}$$

where D represents the moisture diffusivity. Porosity is usually an intrinsic material property that ranges from 1% to 10% for typical polymers.

The calculation of vapor pressure starts with determining the state of moisture in the voids. If the voids contain only vapor and the vapor pressure reaches the saturation point, the saturated moisture density, ρ_g, can be expressed according to the ideal gas law:

$$\rho_g(T) = \frac{p_g(T)}{RM(H_2O)T} \tag{3}$$

where $\rho_g(T)$ is the saturated vapor pressure at a given temperature; the gas constant R = 8.314 J·(mol·K)$^{-1}$, and the water molar mass $M(H_2O)$ = 18 g·mol^{-1}. The vapor pressure can then be evaluated by comparing ρ with ρ_g:

$$p(T) = \begin{cases} \dfrac{RT}{M(H_2O)\phi} \cdot C, & \rho < \rho_g \\ p_g(T), & \rho \geq \rho_g \end{cases} \tag{4}$$

Note that the above equations are still valid if thermal expansion exists due to temperature change. For such a situation, the moisture concentration may change with the change of material volume, which can be calculated by the following relation:

$$dV/dV_0 \approx 1 + 3\alpha\Delta T \tag{5}$$

where ΔT is the temperature difference and α is the coefficient of thermal expansion. Thus, the moisture concentration after expansion becomes:

$$C = dm/dV = \frac{dm}{dV_0}\frac{dV_0}{dV} = C_0(1 - 3\alpha\Delta T) \tag{6}$$

where dm is the moisture mass and dV is the representative element volume.

The whole-field vapor pressure model includes a new field variable ϕ, which stands for the fraction of void volume. Clearly, accurate prediction of vapor pressure relies on void deformation, and the coupling of the vapor pressure model with solid deformation is needed. It is a well-accepted fact that the growth and coalescence of micro-voids in a packaging material will lead to mechanical failures of microelectronic devices (e.g., interface delamination and "popcorn" cracking).

Figure 3 gives examples of using the whole-field vapor pressure model. Based on the modeling results [6], two major factors can be identified: the reflow profile and the substrate thickness. It was found that the reflow profile can be carefully designed to meet the Joint Electron Device Engineering Council (JEDEC) standard and to lower the failure rate. As can be seen in Figure 3(a), under reflow profile a (which has a slow ramp rate), there is a transition point for moisture from binary state to a single vapor state, and the vapor pres-

sure drops due to the loss of moisture as temperature further increases. In comparison, the moisture is always in a binary liquid/vapor state for reflow profile b (which has a fast ramp rate), as shown in Figure 3(b). Consequently, the vapor pressure under reflow profile b is always the same as saturated vapor pressure that increases exponentially with temperature, and may eventually reach the critical stress of the material to cause rupture. It was also discovered that a slight increase of substrate thickness can allow faster moisture escape and thus reduce the possibility of material failures. These findings have been implemented in order to enhance material reliability [6].

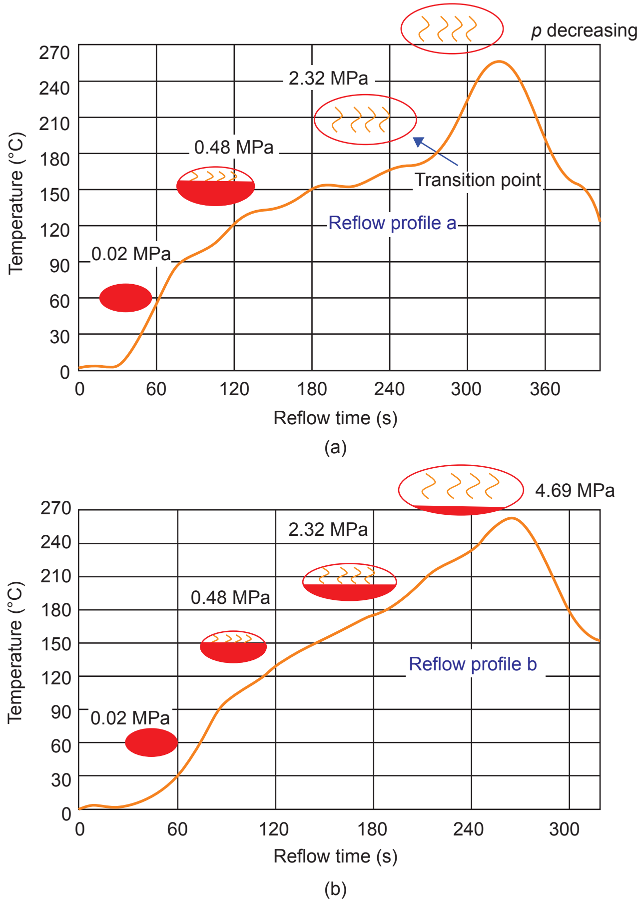

Figure 3. Vapor pressure evolution under different thermal histories [6]. (a) Reflow profile a with "slow" ramp rate; (b) reflow profile b wtih "fast" ramp rate.

2.2 A unified vapor pressure model

In classical moisture diffusion models, the effect of vapor pressure on moisture transport is often overlooked. To consider both water diffusion and vapor flow, a convection-diffusion (CD) model has recently been developed [18, 20], and has also been validated by experimental tests.

In the CD model, a polymer is considered to be a porous medium comprised of a solid matrix and pores. As shown in Figure 4, vapor exists in the micro-voids while liquid water dissolves within the solid matrix. As a result, classical moisture diffusion exists within the solid matrix and convective vapor flow exists through the pore network.

According to Figure 4, the total water density ρ_{m} can be expressed as

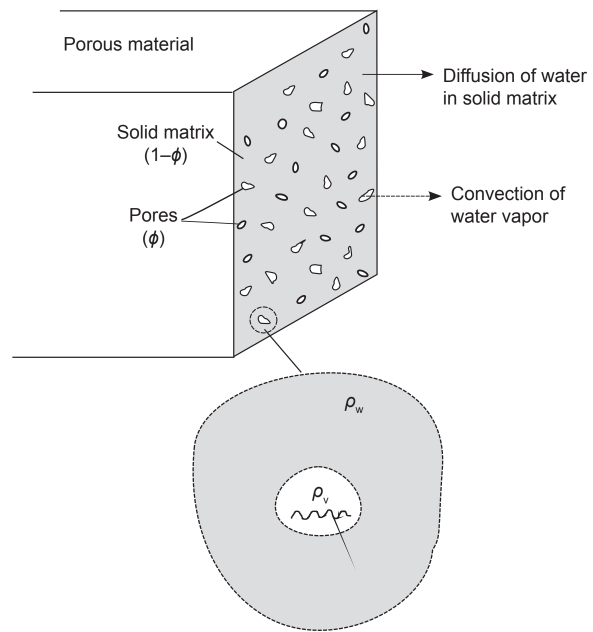

Figure 4. A schematic of the CD model [18].

$$\rho_{\mathrm{m}} = \phi\rho_{\mathrm{v}} + (1-\phi)\rho_{\mathrm{m}} \tag{7}$$

where ρ_{v} is the vapor density and ρ_{w} represents concentrations of dissolved water in the solid matrix. Applying the law of conservation of mass and including both vapor flux and diffusion flux yields the following equation:

$$\phi\frac{\partial\rho_{\mathrm{v}}}{\partial t} + (1-\phi)\frac{\partial\rho_{\mathrm{w}}}{\partial t} = -\nabla\cdot[J(\rho_{\mathrm{v}}) + J(\rho_{\mathrm{w}})] \tag{8}$$

In Eq. (8), the vapor flux is denoted as $J(\rho_{\mathrm{v}})$ and can be described by Darcy's law:

$$J(\rho_{\mathrm{v}}) = -\frac{\rho_{\mathrm{v}}k}{\mu(T)}\nabla p = -\frac{pk}{R_{\mathrm{w}}T\mu(T)}\nabla p \tag{9}$$

where R_{w} is the gas constant for water (461.89 J·(mol·K)$^{-1}$); k is the vapor permeability; and μ is the vapor viscosity dependent on temperature. Generally, permeability k is related to porosity [21] and may have little dependence on temperature [22]. The viscosity of water vapor is known for a given temperature, and this data is available in the *CRC Handbook of Chemistry and Physics*.

The CD model also considers the diffusion flux in the solid matrix, denoted as $J(\rho_{\mathrm{w}})$ in Eq. (8), by using a classical Fick's law:

$$J(\rho_{\mathrm{w}}) = -D(T)\nabla\rho_{\mathrm{w}} \tag{10}$$

where the dissolved water concentration ρ_{w} in a solid matrix can be described with the chemical equilibrium between the liquid and vapor [23, 24], using Henry's law:

$$\rho_{\mathrm{w}} = Bp/p_{\mathrm{g}}(T) \tag{11}$$

where B is a material property. Finally, by substituting Eqs. (9), (10), and (11) into Eq. (8), a vapor pressure model can be obtained:

$$\frac{\phi}{R_{\mathrm{w}}}\frac{\partial(p/T)}{\partial t} + (1-\phi)\frac{\partial(Bp/p_{\mathrm{g}})}{\partial t} = \frac{k}{\mu RT}\nabla\cdot(p\nabla p) + \frac{BD}{p_{\mathrm{g}}}\nabla^2 p \tag{12}$$

Note that this model includes a convective term as well as a diffusion term, which is why it is referred to as the CD model.

Unlike the whole-field vapor pressure model, the CD model solves vapor pressure directly. Once vapor pressure is obtained, moisture concentration can be determined using Eq. (7). Solving vapor pressure directly offers a convenient way to design polymers or polymer composites in situations when vapor pressure must be evaluated, such as in the soldering reflow processes used in the electronic packaging industry. In addition, since vapor pressure is always continuous, there is no need to do normalization for the CD model when dealing with multi-materials. This is a great advantage of this model over the classical diffusion model.

Figure 5 shows an example of using the CD model to analyze desorption data at various temperatures. As shown in this figure, vapor flow can be significant at high temperatures (e.g., up to 30% of moisture loss is from vapor convection), while diffusion can completely dominate the low-temperature behavior of moisture. However, for a device with SH coating, water diffusion may be inhibited at the surface. Thus, vapor flow may be the only way for moisture to transport through the SH coating and enter the device.

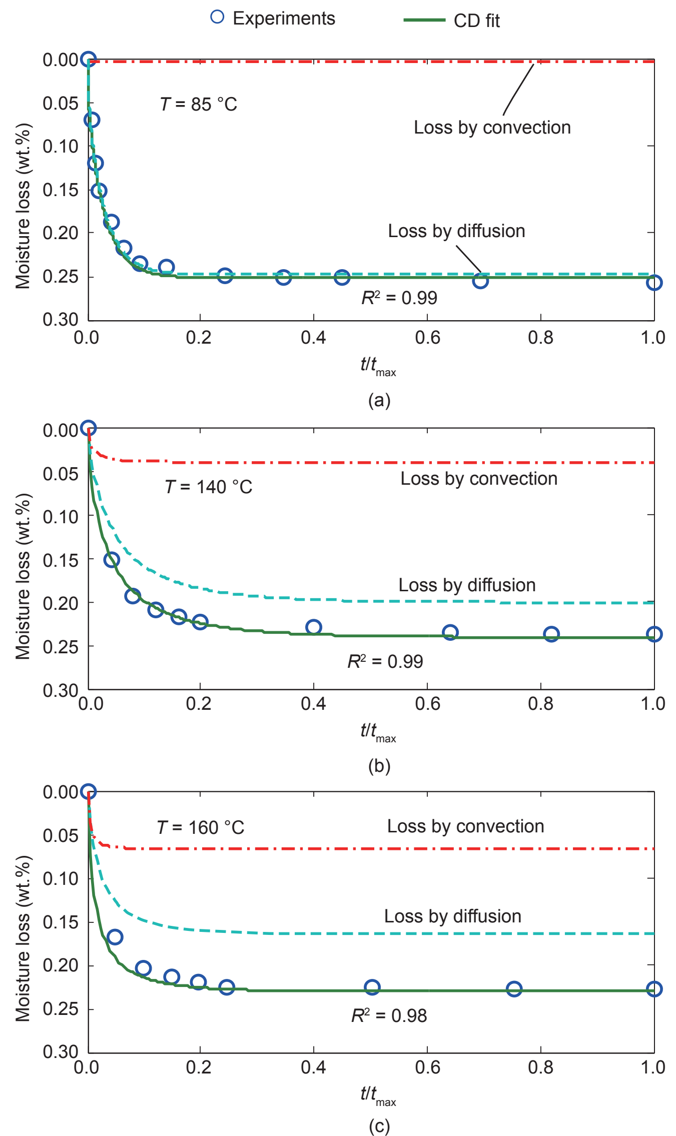

Figure 5. Evolution of vapor flow with temperature rise for desorption tests [18].

2.3 Vapor pressure as external loading

Vapor pressure can be considered as an external loading once the macroscopic delamination is formed and vapor is accumulated in the delaminated area. The progress of interface delamination will be dependent on the magnitude of vapor pressure that changes with time and the delamination volume. For simplicity, uniform vapor pressure can be considered at the delamination interface, whereas the moisture concentrations may differ at different locations. To calculate the average moisture concentration at the delamination interface, a simple equation can be adopted [19]:

$$C^{\mathrm{ave}} = \int_A C\mathrm{d}A / A \tag{13}$$

where A is the delaminated area. In calculating the vapor pressure after delamination by means of the above equation, the concentration C should be replaced by C^{ave}. This method is applicable to both the whole-field vapor pressure model and the CD model. Another method is to explicitly compute the interaction between the water and the solid; this method must deal with the problems of fluid-solid interactions. Microscale fluid-solid interactions can be dealt with using the advanced material point methods [25, 26], in which the surface tension of water and the effect of contact angle can be considered.

2.4 Vapor pressure-induced expansion

It is important to consider vapor pressure-induced expansion when the Young's modulus of a polymeric material becomes a few orders smaller at high temperatures. Vapor pressure-induced expansion can be comparable to thermal expansion and therefore cannot be ignored. To estimate the volume change caused by vapor pressure, the following equation can be used:

$$\frac{\Delta V}{V} = \frac{3(1-2\nu)}{E} p \tag{14}$$

where E is Young's modulus and ν is the Poisson ratio. Substituting E = 500 MPa, ν = 0.3, and p = 2.32 MPa (saturated vapor pressure at 220 °C) yields 5.558×10^{-3} for a typical underfill material [19]. The equivalent thermal expansion coefficient is approximately 41 ppm·°C^{-1} based on a temperature loading from 175 °C to 220 °C [19]. It is obvious that if a reduced Young's modulus is considered, the deformation mismatch could be very significant. This simple case demonstrates the importance of coupling vapor-pressure-induced expansion for the accurate prediction of solid deformation.

3 Effects of SH surface coating

Both the whole-field vapor pressure model and the CD model infer that high vapor pressure can be avoided by preventing moisture uptake, namely when C or ρ_w becomes zero. This situation can be achieved by applying a water-repelling coating or encapsulant to the targeted device before exposing it to a humid environment.

Many types of encapsulants have been used for moisture

prevention, including silicone polyimides and polyxylylene (parylene) [27]. It has been reported that the application of encapsulants protects electronic components from high-temperature humidity bias (THB) condition, thermal shock, and temperature cycles during real-life applications. Moreover, the encapsulant coating can prevent the infusion of mobile ion contaminations and moisture, and increase the long-term reliability of nonhermetic packages [28, 29]. It was also found that using an SH surface yielded much better protection for microelectromechanical systems (MEMS) from moisture damage.

Two general rules exist for designing an SH coating: One is to minimize the free energy and the other is to increase the surface roughness. Surface morphology or roughness plays a critical role in obtaining SH properties. The relation between the surface roughness and the contact angle can be described by the Wenzel equation [30]:

$$\cos\theta_{\mathrm{A}} = r\cos\theta_{\mathrm{Y}} \tag{15}$$

where θ_A is the apparent contact angle; r is the roughness index; and θ_Y is the contact angle when r = 1.0 (which corresponds to a flat surface). Obviously, the goal of designing an SH surface is to increase the roughness (r) and then the contact angle. However, the Wenzel state is typically insufficient to achieve a higher contact angle (e.g., > 150°). The apparent contact angle yielded by a nanocomposite coating is closely related to the solid surface fraction (f), which can be described by the Cassie equation [31]:

$$\cos\theta_{\mathrm{A}} = -1 + f\left(\cos\theta_{\mathrm{Y}} + 1\right) \tag{16}$$

Figure 6 shows the procedures required to achieve an SH surface using a silica/epoxy nanocomposite to protect microelectronic components [11]. Most nanosilica particles (100 nm, 10 wt.%) in the epoxy mixture were located underneath the top layer of epoxy after spin-coating of the mixture on the microelectronic samples. In order to have the nanosilica exposed from the epoxy for increased surface roughness, oxygen reactive ion etching (RIE) can be used to etch out epoxy molecules using different etching durations, as shown in Figure 6(a). Next, long-chain fluorocarbon silane is coated onto the nanosilica-exposed top surface in order to further reduce the surface energy. As shown in Figure 6(b), the primary anchoring site for silane molecules is on the hydroxyl group on the surface of the nanosilica. Figure 7 shows the changes in surface roughness due to different etching durations. The surface roughness and solid surface fraction are significantly increased by exposing the tops of the silica particles and forming a densely packed layer. More air is trapped at the water and composite interface, forming a highly hydrophobic system, with $\theta_A \approx 161°$ and hysteresis less than 2°. The measurement of the contact angle was taken after the coating was fully cured (note that the degree of cure may be roughly measured by solvent rub testing). Experiments were conducted to measure the resistance and leakage current of a triple-track resistor with an SH epoxy/silica coating under the conditions of 85 °C/85% relative humidity (RH) and a constant direct current (DC) bias of 13.4 V [11]. The results showed less degradation of the resistance and leakage current in coated samples compared to samples that were uncoated or samples that were coated with a common encapsulant lacking SH properties. However, this study did not report the weight gain for the extended time, and the long-term effectiveness of an SH coating is unclear.

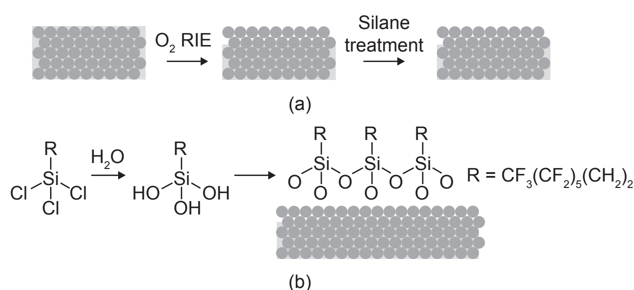

Figure 6. Illustration of the SH surface synthesis process. (a) O_2 plasma etching and silane treatment; (b) hydrophobic treatment with perfluorooctane sulfonate (PFOS) on a nanocomposite surface [11].

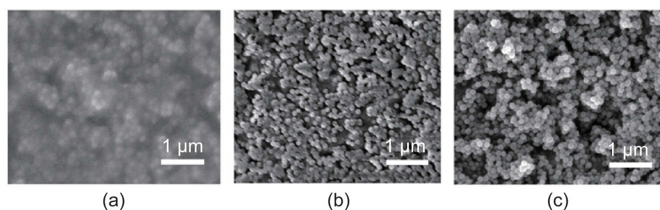

Figure 7. Surface roughness changing with etching time [11].

4 Moisture uptake after SH coating

To further verify the effectiveness of SH coating under various conditions, experimental tests were carried out to measure the failure rates of coated materials during the soldering reflow tests after moisture absorption [16]. For comparison, both as-received samples and SH-thin-film-coated samples were tested. Quad flat package (QFP) was used. Two different moisture conditions were applied. One moisture condition involved the immersion of the samples into water at 60 °C. The other condition involved placing the samples in a humidity chamber with 60 °C/85% RH. An extended testing time of more than 192 hours was applied. It was found that the coated samples were well-protected in the first moisture condition (immersion into water), with very insignificant moisture uptake. However, the effect of the SH coating seemed to disappear under the moisture condition of 60 °C/85% RH; almost the same amount of moisture uptake was measured for the coated and uncoated samples. The reflow test after moisture absorption confirmed that the coated package would only have a higher survival rate than the uncoated package when they were both immersed in water. For the condition of 60 °C/85% RH, there was no difference in the failure rates for the coated and uncoated samples. It can be implied from these observations that coating materials that may be very effective in repelling liquid water may not stop the uptake of water vapor. This finding is schematically shown in Figure 8.

To explain the phenomenon shown in Figure 8, we consider that two diffusion mechanisms may exist within the coated materials: moisture transfer across the SH surface and mois-

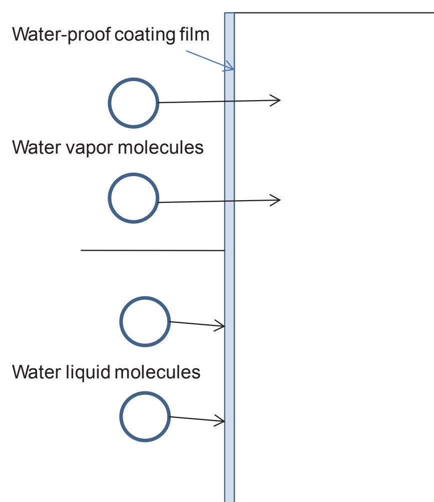

Figure 8. Schematic picture for a hydrophobic coating film that fails to prevent water vapor penetration [16].

ture transfer through bulk. Generally speaking, moisture transfer through bulk is quite well understood with Fickian kinetics. However, the diffusion mechanism across the surface, particularly for an SH surface, may be more complex and could depend strongly on the vapor pressure and the chemistry of the materials. It is believed that vapor pressure at the SH surface could be the key to fully understanding the surface diffusion mechanism that was observed in the experiments.

5 Discussion and conclusions

This paper presented two different theoretical models for vapor pressure prediction within electronic materials: the whole-field vapor pressure model and the CD model. The whole-field vapor pressure model combines Fickian diffusion with the micromechanics of water vapor in micro-voids in order to estimate the vapor pressure, while the CD model incorporates Fickian diffusion, vapor convection, and the chemical equilibrium of a liquid-vapor mixture in order to form a unified vapor pressure model. In spite of the differences between them, both methods can be further coupled with solid deformation by considering the vapor pressure-induced deformation. It can be shown that the vapor pressure prediction is crucial for investigating the total mechanical responses of materials in high-temperature and high-humidity environments. For the CD model, it has been shown that vapor flow may be significant at high temperatures (e.g., reaching 29% of the total moisture transport at 160 °C). Compared to diffusion-only or convection-only models, the CD model is able to fit the experimental data accurately by combining both diffusion and convection mechanisms at various temperatures. For polymer composites that are subject to rapid heating at high temperatures, our numerical study shows that a high heating rate could generate a very high vapor pressure (around 6.5 MPa), which may cause reliability issues within the material.

To enhance device reliability in a humid environment, an SH nanocomposite coating was developed and tested under various moisture conditions. It was observed that the SH coating, which is water-repelling, may not be effective in protecting the material underneath from water vapor. Although diffusion models have been developed over many decades, the underlying mechanism of diffusion through an SH coating is still an open question. Since vapor pressure can be altered by microscale surface roughness, accurate estimation of vapor pressure on an SH surface could be extremely important to determine whether the SH coating is vapor-proof or not. Based on this study, it is necessary to develop a multi-scaled vapor pressure model that is able to consider the nano structure of SH coatings.

Acknowledgement

The authors would like to acknowledge the support of the National High-Tech Research and Development Program of China (863 Program) (2015AA03A101).

Compliance with ethics guidelines

Xuejun Fan, Liangbiao Chen, C. P. Wong, Hsing-Wei Chu, and G. Q. Zhang declare that they have no conflict of interest or financial conflicts to disclose.

References

1. X. Q. Shi, Y. L. Zhang, W. Zhou, X. J. Fan. Effect of hygrothermal aging on interfacial reliability of silicon/underfill/FR-4 assembly. *IEEE T. Compon. Pack. T.*, 2008, 31(1): 94–103
2. X. J. Fan, E. Suhir. Moisture Sensitivity of Plastic Packages of IC Devices. New York: Springer, 2010.
3. X. J. Fan, G. Q. Zhang, W. D. van Driel, L. J. Ernst. Interfacial delamination mechanisms during soldering reflow with moisture preconditioning. *IEEE T. Compon. Pack. T.*, 2008, 31(2): 252–259
4. W. D. van Driel, M. A. J. van Gils, X. J. Fan, G. Q. Zhang, L. J. Ernst. Driving mechanisms of delamination related reliability problems in exposed pad packages. *IEEE T. Compon. Pack. T.*, 2008, 31(2): 260–268
5. B. Xie, X. J. Fan, X. Q. Shi, H. Ding. Direct concentration approach of moisture diffusion and whole-field vapor pressure modeling for reflow process-Part I: Theory and numerical implementation. *J. Electron. Packag.*, 2009, 131(3): 031010.1–031010.7
6. B. Xie, X. J. Fan, X. Q. Shi, H. Ding. Direct concentration approach of moisture diffusion and whole-field vapor pressure modeling for reflow process-Part II: Application to 3D ultrathin stacked-die chip scale packages. *J. Electron. Packag.*, 2009, 131(3): 031011.1–031011.6
7. L. S. Zhu, J. Zhou, X. J. Fan. Rupture and instability of soft films due to moisture vaporization in microelectronic devices. *Computers, Materials & Continua*, 2014, 39(2): 113–134
8. Y. H. Xiu, L. B. Zhu, D. W. Hess, C. P. Wong. Superhydrophobic durable silica thin films from sol-gel processing for the application in antistiction of MEMS devices. *Abstracts of Papers of the American Chemical Society*, 2006: 231
9. Y. Liu, W. Lin, Z. Lin, Y. Xiu, C. P. Wong. A combined etching process toward robust superhydrophobic SiC surfaces. *Nanotechnology*, 2012, 23(25): 255703
10. Y. Liu, Z. Lin, W. Lin, K. S. Moon, C. P. Wong. Reversible superhydrophobic-superhydrophilic transition of ZnO nanorod/epoxy composite films. *ACS Appl. Mater. Interfaces*, 2012, 4(8): 3959–3964
11. Y. Liu, Z. Lin, K. S. Moon, C. P. Wong. Superhydrophobic nanocomposite coating for reliability improvement of microelectronics. *IEEE Trans. Compon. Packag. Manuf. Tech.*, 2013, 3(7): 1079–1083
12. Y. H. Xiu, Y. Liu, B. Balu, D. W. Hess, C. P. Wong. Robust superhydrophobic surfaces prepared with epoxy resin and silica nanoparticles. *IEEE Trans. Compon. Packag. Manuf. Tech.*, 2012, 2(3): 395–401

13. Y. Liu, Y. Xiu, D. W. Hess, C. P. Wong. Silicon surface structure-controlled oleophobicity. *Langmuir*, 2010, 26(11): 8908–8913
14. X. J. Feng, L. Jiang. Design and creation of superwetting/antiwetting surfaces. *Adv. Mater.*, 2006, 18(23): 3063–3078
15. L. Gao, T. J. McCarthy. The "lotus effect" explained: Two reasons why two length scales of topography are important. *Langmuir*, 2006, 22(7): 2966–2967
16. X. J. Fan, S. W. R. Lee, Q. Han. Experimental investigations and model study of moisture behaviors in polymeric materials. *Microelectron. Reliab.*, 2009, 49(8): 861–871
17. E. H. Wong, S. W. Koh, K. H. Lee, K.-M. Lim, T. B. Lim, Y.-W. Mai. Advances in vapor pressure modeling for electronic packaging. *IEEE Trans. Adv. Packag.*, 2006, 29(4): 751–759
18. L. Chen, H. W. Chu, X. J. Fan. A convection-diffusion porous media model for moisture transport in polymer composites: Model development and validation. *J. Polym. Sci. Pol. Phys.*, 2015, 53(20): 1440–1449
19. X. J. Fan, J. Zhou, G. Q. Zhang, L. J. Ernst. A micromechanics-based vapor pressure model in electronic packages. *J. Electron. Packag.*, 2005, 127(3): 262–267
20. J. Adams, L. Chen, X. J. Fan. Vapor pressure prediction for stacked-chip packages in reflow by convection-diffusion model. In: *Proceedings of the 16th International Conference on Thermal, Mechanical and Multi-Physics Simulation and Experiments in Microelectronics and Microsystems (EuroSimE)*. Budapest, Hungary, 2015
21. Y. Wu, N. Katsube. A thermomechanical model for chemically decomposing composites—I. Theory. *Int. J. Eng. Sci.*, 1997, 35(2): 113–128
22. R. M. Sullivan. The effect of water on thermal stresses in polymer composites. *J. Appl. Mech.*, 1996, 63(1): 173–179
23. G. K. van der Wel, O. C. G. Adan. Moisture in organic coatings—A review. *Prog. Org. Coat.*, 1999, 37(1–2): 1–14
24. H. B. Hopfenberg, H. L. Frisch. Transport of organic micromolecules in amorphous polymers. *J. Polym. Sci., Part B. Polym. Lett.*, 1969, 7(6): 405–409
25. L. Chen, J. H. Lee, C. F. Chen. On the modeling of surface tension and its applications by the Generalized Interpolation Material Point Method. *CMES-Comp. Model. Eng.*, 2012, 86(3): 199–224
26. L. Chen. Using the generalized interpolation material point method for fluid-solid interactions induced by surface tension (Doctoral desseration). Fairbanks, AK: University of Alaska Fairbanks, 2013
27. C. P. Wong. High-performance silicone gel as IC device chip protection-cure study and electrical reliability. *Abstracts of Papers of the American Chemical Society*, 1988: 102
28. R. G. Mancke. A moisture protection screening test for hybrid circuit encapsulants. *IEEE Trans. Compon. Hybrids Manuf. Technol.*, 1981, 4(4): 492–498
29. J. L. Wu, R. T. Pike, C. P. Wong, N. P. Kim, M. H. Tanielian. Evaluation and characterization of reliable non-hermetic conformal coatings for microelectromechanical system (MEMS) device encapsulation. *IEEE Trans. Adv. Packag.*, 2000, 23(4): 721–728
30. R. N. Wenzel. Resistance of solid surfaces to wetting by water. *Ind. Eng. Chem.*, 1936, 28(8): 988–994
31. A. B. D. Cassie, S. Baxter. Wettability of porous surfaces. *Trans. Faraday Soc.*, 1944, 40: 546–551